

Localization and Anomalous Transport in a 1-D Soft Boson Optical Lattice

A. K. Tuchman, W. Li, H. Chien, S. Dettmer, M. A. Kasevich

Physics Department, Stanford University, Stanford CA, 94305

(Dated: September 23, 2018)

Abstract

We study the dynamics of Bose-Einstein condensed atoms in a 1-D optical lattice potential in a regime where the collective (Josephson) tunneling energy is comparable with the on-site interaction energy, and the number of particles per lattice site is mesoscopically large. By directly imaging the motion of atoms in the lattice, we observe an abrupt suppression of atom transport through the array for a critical ratio of these energies, consistent with quantum fluctuation induced localization. Directly below the onset of localization, the frequency of the observed superfluid transport can be explained by a phonon excitation but deviates substantially from that predicted by the hydrodynamic/Gross-Pitaevskii equations.

Coherent control of the collective dynamics of macroscopic quantum systems is currently of great interest due to possible applications in quantum measurement and information science [1, 2]. For example, coherent manipulation of superconducting currents in Josephson junction circuits has led to the realization of high- Q electronic qubits for quantum logic devices [3]. Similarly, manipulation of the superfluid properties in atomic systems, such as with BECs in optical lattices, may soon provide a realization of de Broglie wave interferometers which perform below the shot-noise limit [4].

At zero temperature, the physical characteristics of coupled superconducting/superfluid reservoirs are determined by two competing energies: the kinetic energy associated with tunneling between sites (E_J), and the on-site interaction energy (E_C), resulting from (repulsive) inter-particle interactions [5, 6]. Specifically, for a BEC in an optical lattice system $E_J \equiv N\gamma$, where N is the number of atoms in a lattice site and γ is the inter-site tunneling energy, and $E_C \equiv g\beta$, where $g\beta$ is the mean-field energy. The nature of the many-body ground state in the lattice array is governed by the ratio $\Gamma \equiv E_C/E_J \equiv g\beta/N\gamma$, which can be divided into three regimes. For $\Gamma \ll 1$, the system exhibits global superfluidity and long-range phase order. As Γ approaches 1, interactions lead to a frustration of long-range phase order and a corresponding reduction of the single reservoir number variance δN , with $\delta N \sim (N\gamma/g\beta)^{1/4}$. When $\Gamma \sim 1$, the system undergoes a transition to an insulating regime where number fluctuations are strongly suppressed ($\delta N < 1$) for commensurate filling. For translationally invariant lattice arrays, this defines the Mott-insulating regime (MI) [7, 8]. This system has been shown to map onto 1-D superconducting chains, which demonstrate a Kosterlitz-Thouless transition [9].

Previously, interferometric techniques have been used to study the ground state properties of BECs in optical lattices forming 1-D arrays with high filling factor in the regime $\Gamma > 1$ [10]. This work demonstrated that, for the system studied, interferometric measurements do not have the specificity to reveal possible abrupt changes in the many-body state of the system as the Mott-insulating regime is reached [11]. However, recent theoretical work has shown that transport measurements in the regime $\Gamma \sim 1$ are expected to provide additional insights into the superfluid properties of the array [12]. Similar transport measurements have previously been used to study the superfluid properties of arrays in the semiclassical regime, $\Gamma \ll 1$, and have observed both superfluid transport [13] as well as damping. Dissipation has been attributed primarily to either dynamical instabilities [14] or quantum fluctuation

effects [15, 16], depending on the experimental parameters. Both of these mechanisms make it difficult to observe finite amplitude transport for systems in their ground state at deep lattice depths, even for $\Gamma < 1$.

In this work, however, we observe residual coherent transport in this dissipative regime, which we attribute to the presence of anomalous phonon excitations. We study this transport through direct observation of atom motion across a 1-D lattice array superimposed on a weaker harmonic potential. We observe a crossover from coherent oscillatory behavior to localization as we vary the strength of the coupling between adjacent lattice sites. We attribute this localization to the role of quantum fluctuations in driving the formation of strongly correlated, mesoscopic insulating states with lattice site atom number occupation, $N \sim 100$. We support this interpretation by observing the cessation of macroscopic tunnelling to occur when $\Gamma \sim 1$, the same critical relation found in analogous Josephson junction experiments [17]. Furthermore, we rule out localization due to known semiclassical effects.

The Bose-Hubbard Hamiltonian is expected to provide an accurate theoretical description of a lattice array of bosonic atoms [18]. Written in terms of the on-site single particle creation and annihilation operators \hat{a}_i^\dagger and \hat{a}_i :

$$H = -\gamma \sum_{\langle i,j \rangle} \hat{a}_i^\dagger \hat{a}_j + \sum_i \frac{1}{2} g \beta_i \hat{a}_i^\dagger \hat{a}_i^\dagger \hat{a}_i \hat{a}_i + \sum_i V_i \hat{a}_i^\dagger \hat{a}_i \quad (1)$$

where $V_i = \Omega i^2$ is the external potential due to the harmonic magnetic trap, the subscript i denotes the i th lattice site, and $g = 4\pi\hbar^2 a/m$ (a is the repulsive s-wave scattering length and m is the atomic mass). β_i and γ are determined from integrals over single particle wavefunctions [19], and can be precisely, experimentally controlled by raising and lowering the intensity of the optical lattice in order to vary Γ .

In our experiments, we investigate the response of the lattice ground state to sudden shifts in the position of the harmonic potential used to initially create the condensate. Exact theoretical predictions using Eq. 1 for the ensuing array dynamics are difficult for our experimental conditions due to the large Hilbert space needed to model the system. Nevertheless, we gain intuition into the dynamic behavior by considering limiting regimes. For static potentials and translationally invariant arrays, a second order quantum phase transition from a superfluid to a MI phase is predicted to occur at $\Gamma \sim 1$ [7, 9, 20, 21]. At this point the many-body wavefunction localizes to a product of states with nearly

quantized atom number at each lattice site for commensurate lattice filling. Such states lack macroscopic phases, and thus, we expect suppression of Josephson-like transport of atoms through the array when an external driving force is applied. On the other hand, just below the transition, particle fluctuations $1 < \delta N \ll N^{1/2}$ are sufficient to define an average macroscopic phase and induce superfluidity, even for large filling factors.

Inclusion of the external harmonic potential (as in Eq. 1) complicates the analysis [18, 22, 23, 24]. For deep lattices, where $\Gamma > 1$ across the entire array, mean-field analysis predicts isolated Mott domains of incommensurate filling with local incompressible regions but does not demonstrate the vanishing global compressibility indicative of a true phase transition [24]. These domains have been recently observed in Refs. [25, 26]. For shallower lattices, regions near the edges of the array can locally fulfill the Mott-insulator condition, while the central lattice sites remain in the superfluid regime. We expect the formation of these insulating barriers to substantially alter the dynamics of the superfluid confined in the interior regions.

For a given lattice strength, U , we determine the values of $g\beta_i$ and N_i using the following two-step approach. First, we numerically solve the 3-D Gross-Pitaevskii equation (GPE) [27] for a single lattice site (neglecting tunneling between adjacent lattice sites) to determine the spatial wavefunction associated with the individual lattice sites as a function of the strength of the lattice potential and the number of atoms in the well. This allows determination of the chemical potential μ_i and effective value of $g\beta_i$ [28, 29]. Analytic expressions for these quantities can be obtained in the limit where the kinetic energy is negligible. For our parameters, the analytic expressions agree to within 10% with numerical estimates that do not neglect kinetic energy. Next, we estimate the equilibrium distribution of the mean occupancy of each lattice site across the array by equating the chemical potentials associated with each site, subject to the constraint that the total number of atoms sums to a fixed value. We obtain analytic expressions if we neglect kinetic energy associated with tunneling, which is an excellent approximation for the lattice depths explored in this work. For $U = 50 E_R$, the central lattice site contains roughly 120 atoms, with a $1/e$ radius of 19 lattice sites, where $g\beta/\hbar \sim 17$ rad/s and $\gamma/\hbar \sim 0.6$ rad/s.

Accurate determination of Γ (Fig. 1) further hinges on measurement calibration of atom number and lattice depth. We infer the total number of atoms in the trapped condensate from an absorptive image of the atomic array. We measure the lattice depth in three

independent ways. First, we determine the lattice depth through direct observation of the harmonic oscillation frequency in each well: we measure atoms lost from the lattice via parametric heating as a function of the modulation frequency of a small amplitude perturbation to the position of the potential minimum. Second, we measure the period of Kapitza-Dirac diffraction by suddenly turning on the lattice [30]. Finally, we directly measure γ at weak lattice depths ($U < 10 E_R$) by observing the amplitude of the oscillation induced by an applied transient phase gradient [31]. In particular, a phase shift (quasi-momentum) $\delta\phi = \pi/2$, induces an oscillation with an amplitude (in lattice units) equal to $\sqrt{2\gamma/\Omega}$ [32]. These experimental techniques determine the lattice calibration with an uncertainty of $\pm 8\%$, which agrees with the calculated lattice depth based on measured parameters to within 20%.

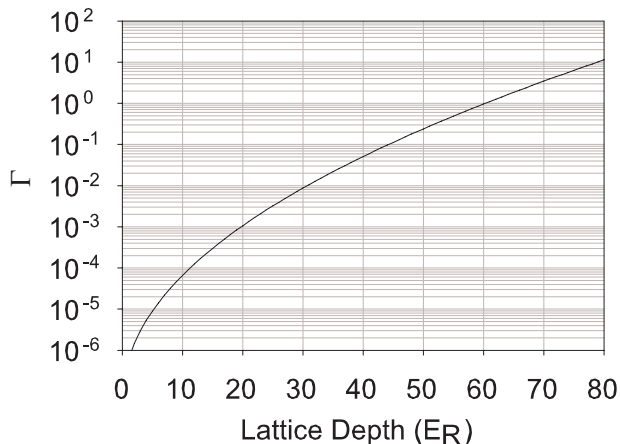


FIG. 1:

$\Gamma \equiv E_C/E_J \equiv g\beta/N\gamma$ is calculated as a function of lattice depth. For a translationally invariant lattice system, $\Gamma \sim 1$ denotes the onset of a Mott-Insulating regime.

Our experimental apparatus is described in detail in Ref. [10] and begins with 10^8 laser cooled ^{87}Rb atoms loaded into a time-orbiting potential (TOP) trap. We use both TOP and forced radio frequency evaporative cooling to generate nearly pure condensates with $4 \pm 1 \times 10^3$ atoms, optically pumped into the $F = 2$, $m_F = 2$ state. We estimate $T/T_c \sim 0.27$ before the lattice is turned on (T is the temperature and T_c the BEC transition temperature). After the BEC phase transition, we adiabatically relax the magnetic trap, thereby increasing

the condensate's size and decreasing its density. This results in a radial trapping frequency of $\omega_{\perp} = 70$ rad/s and $\omega_z = 195$ rad/s, corresponding to $\Omega/\hbar = 4.2$ rad/s ($\Omega = 2.1 \times 10^{-4} E_R$). A retro-reflected laser beam in the vertical direction at a wavelength $\lambda = 840$ nm is superimposed over the condensed atom cloud to create a 1-D lattice potential. The light is focussed to a $1/e$ intensity radius of $50 \mu\text{m}$ and is far-detuned to the red from the 780 nm optical resonance of ^{87}Rb . This creates a standing wave which forms a periodic array of potential wells spaced by $\lambda/2$. Atoms occupy lattice sites at the anti-nodes of the sinusoidally varying optical potential. The lattice also provides additional transverse confinement of the atoms. For example, at $U = 50 E_R$, the characteristic trap frequencies are 842 rad/s (transverse) and 3.1×10^5 rad/s (longitudinal).

We slowly increase the intensity of the lattice laser (in a time of 200 ms) to minimize non-adiabaticity in the state preparation. We note that this ramp may not be strictly adiabatic for the deeper lattice depths used in this work [33, 34]. In order to study the transport properties of atoms through the array, we suddenly shift the harmonic potential minimum and stroboscopically observe the ensuing motion of the center-of-mass of the array (using destructive absorptive imaging techniques). We shift the harmonic potential by pulsing on a weak vertical magnetic field. The resulting translation, Δ , to the minimum induces a chemical potential offset, $E = 4\Delta\Omega/\lambda$, between adjacent wells, which drives subsequent array dynamics.

We investigate three regimes of lattice transport: $\Gamma \ll 1$, $\Gamma < 1$ and $\Gamma \geq 1$. In order to tie in with previous work [13, 15], we first explore the superfluid regime for low lattice depths ($\Gamma \ll 1$) where the semiclassical hydrodynamic equations are well suited. Transport oscillation frequencies closely follow a scaled harmonic magnetic trap frequency, $\omega = \omega_0 \sqrt{m/m^*}$ with an effective mass, $m/m^* = \gamma\pi^2/2E_R$, determined by the lattice depth [35]. We characterize the observed oscillations through their amplitude and frequency, determined by non-linear least squares fits to the oscillation time sequences [$z(t) = Ae^{-tb/2m^*} \cos(\omega t)$, where A denotes the oscillation amplitude and b the damping coefficient]. In Fig. 2A, we see good correlation of our observed frequencies with semiclassical theory. Ground state coherent transport in this regime is also contingent on the trap displacement being sufficiently small so that an unstable regime is avoided.

If the trap displacement is too large, the system enters a dynamically unstable regime, where small perturbations around a plane wave grow exponentially in time [14]. This is

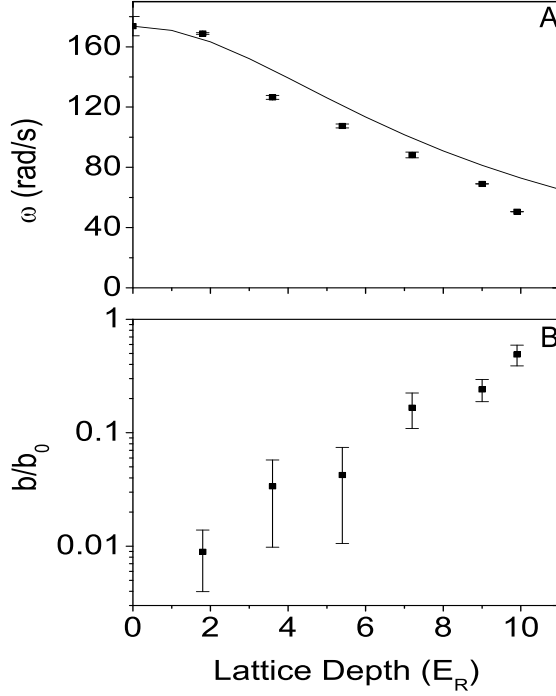


FIG. 2:

(A) Center-of-mass oscillation frequency vs. lattice depth for $\Delta = 3.5 \mu\text{m}$. Solid line is solution to semiclassical hydrodynamic equations. (B) Damping of center-of-mass oscillation vs. lattice depth. b/b_0 notation is adopted for comparison with Ref. [15], where $b_0 \equiv 2m\omega_0$, and ω_0 is the magnetic harmonic trap frequency.

expected to occur after a critical displacement, $\Delta_{\text{crit}} = \lambda/2\sqrt{2\gamma/\Omega}$, where a $\pi/2$ phase difference accumulates between adjacent wells [32]. In this regime, dissipation is expected to lead to rapid frustration of coherent tunneling. For $\Delta = 6.4 \mu\text{m}$, the largest displacement used in this work, this occurs for $U > 10 E_R$ (see Fig. 3).

The data shown in Fig. 2, however, demonstrates significant damping, despite being taken with $\Delta < \Delta_{\text{crit}}$. Furthermore, for this data $\gamma \gg E$, indicating that the width of the lowest band is greater than the energy offset induced between wells (see Fig. 3). Thus, we also do not expect localization related to Bloch oscillations. One possible explanation for the damping seen in Fig. 2B is effects due to quantum fluctuations, predicted to occur even at low lattice depths [23, 36]. This effect has recently been suggested as a potential mechanism

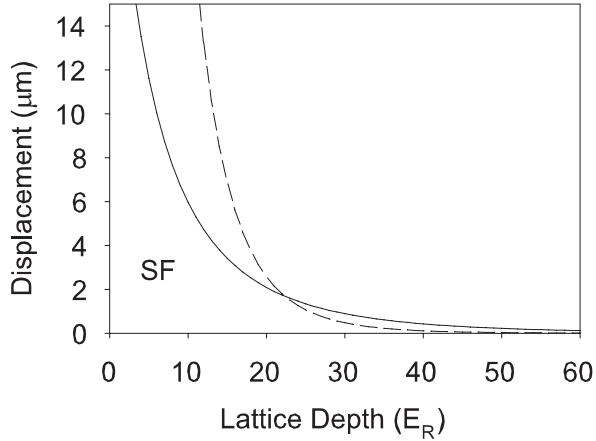


FIG. 3:

Critical displacement, Δ_{crit} , as predicted by the GPE, is plotted as a function of lattice depth, shown with a solid line. Above the solid line this semiclassical picture predicts a dynamically unstable, dissipative regime, and below the line, superfluid transport (SF) is expected. The dashed line indicates the condition where $\gamma = E$. For $E > \gamma$ and weak interactions, lattice dynamics are governed by Bloch oscillations.

for experimentally observed damping in Ref. [15]. We note that the damping observed in Ref. [15] is significantly greater than what we observe, however, in that system, lattice site occupation is on the order of unity. Other possible explanations for our observed damping include finite temperature effects [37].

For $\Gamma < 1$ we observe higher frequency oscillations which emerge on top of the overdamped slower oscillations. Fig. 4A shows a slow oscillation in the underdamped region with $\omega = 88.2 \pm 1.9$ rad/s at $U = 7.2 E_R$. Fig. 4B displays the emergence of a faster oscillation with $\omega = 149.9 \pm 5.8$ rad/s, taken at $U = 10.8 E_R$, where the non-linear fit requires an added linear term to account for the initial slope. We continue to observe high frequency transport oscillations as the lattice is increased for $U < 50 E_R$, as shown in Fig. 5A. We rule out the possibility of these high frequency oscillations being Bloch oscillations since ω is independent of Δ , which determines the energy offset between adjacent wells.

The presence of these oscillations cannot be explained within the ground state semiclassical picture, since the observed frequencies are much greater than those expected from

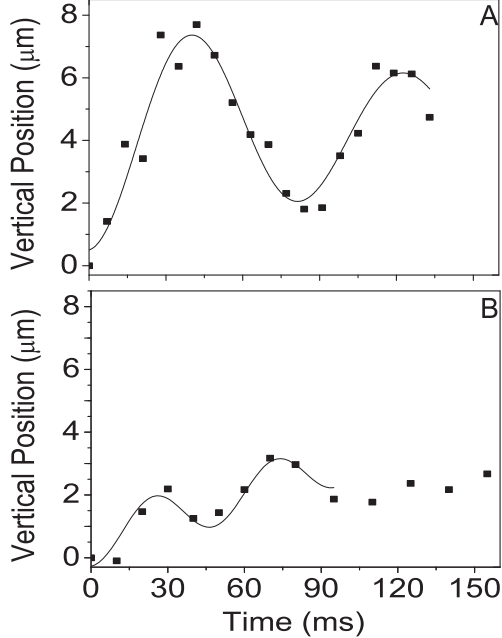


FIG. 4:

Center-of-mass oscillations with $\Delta = 3.5 \mu\text{m}$ are shown for (A) the underdamped regime, with $\omega = 88.2 \pm 1.9 \text{ rad/s}$ for $U = 7.2 E_R$ and (B) the overdamped regime, with $\omega = 149.9 \pm 5.8 \text{ rad/s}$, taken at $U = 10.8 E_R$.

the hydrodynamic equations (see dashed line in Fig. 5A) [35]. In addition, our observed frequencies cannot be explained by using standard approximations to include the role of quantum fluctuations in ground state transport. Recent theoretical approaches using the Truncated Wigner approximation (TWA) have shown that quantum fluctuations tend to reduce transport frequencies in the overdamped regime and to increase damping [23].

We expect, however, that the observed frequencies in this regime should be related to the characteristic frequencies for phonon excitations. An array phonon frequency can be determined for an effective phonon wave-vector, q_{eff} , which characterizes the array coherence length. We infer q_{eff} from the phonon dispersion relation for a uniform lattice $\hbar\omega_q = \sqrt{4\gamma \sin^2(\frac{q\lambda}{4})[2N_i g\beta + 4\gamma \sin^2(\frac{q\lambda}{4})]}$ [6]. We find that for suitably deep lattice depths (near the expected MI cross-over), our observed frequencies correspond to phonon excitations with $4\pi/q_{\text{eff}}\lambda = 4$ lattice sites, as seen in Fig. 5A. It is interesting to note that this phonon frequency also corresponds to the generalized Josephson frequency associated with a 2-well system. As described earlier, the complexity of the Hilbert space of our system makes achieving a quantitative theoretical prediction for q_{eff} very difficult. However, our empirical

observation of an effective phonon excitation length (4 sites), much less than the full spatial extent of the atomic cloud (19 sites), may be due to the emergence of MOT domains in the outer wells [25, 26]. For shallower lattice depths (in the regime shown in Fig. 5A) we observe frequencies which are consistent with longer range phonon modes, possibly due the effective array coherence length increasing with reduced Γ [38].

We note that for these lattice depths, our experiments probe the ill-understood regime where the semiclassical (Gross-Pitaevskii/hydrodynamic) equations become dynamically unstable (see Fig. 3). In this regime, for example, the Bogoliubov dispersion relations have imaginary solutions and unconventional normalization [39], and thus, the TWA is unreliable. It has been shown that the exact quantum dynamics of a dynamically unstable system diverge (logarithmically with N) from the classical trajectories [40, 41], which further complicates the analysis of our excited state transport.

For $\Gamma \sim 1$ we observe an abrupt cessation of superfluid transport. The oscillation amplitude falls to zero at a critical value for the lattice depth corresponding to $\Gamma \sim 1$ (Fig. 5B), consistent with the expected superfluid-MI transition [9, 21] (at $U = 49 E_R$, $\Gamma = 0.21$ with an error range of $0.09 < \Gamma < 0.52$ determined, predominantly, by our experimental uncertainty in lattice calibration). Fig. 5B (see lower inset) illustrates the oscillation induced by a shift ($\Delta = 6.4 \mu\text{m}$) in the harmonic potential at a lattice depth of $U = 47 E_R$ and is contrasted with localization observed for the same displacement at $U = 54 E_R$ (see upper inset). The observed threshold is independent of the lattice displacement (within our experimental limits). Additionally, above the transition, the atoms are observed to localize immediately after the shift in position of the harmonic potential, as illustrated in the inset to Fig. 5B. These observations explicitly rule out other localization mechanisms – such as macroscopic quantum self-trapping [42, 43] or dynamical instabilities [32] – where the localization depends on the initial displacement, or manifests itself only after the array dynamically evolves following the displacement (in the case of dynamical instabilities).

In conclusion, we have used the presence of anomalous phonon excitations to probe atom transport deep in the dissipative regime. This regime has been previously inaccessible using ground state array transport. We observe localization to occur at the critical value $\Gamma \sim 1$, which suggests localization due to quantum fluctuation effects. This work raises the possibility for further control of macroscopic quantum coherence, even in excited state systems.

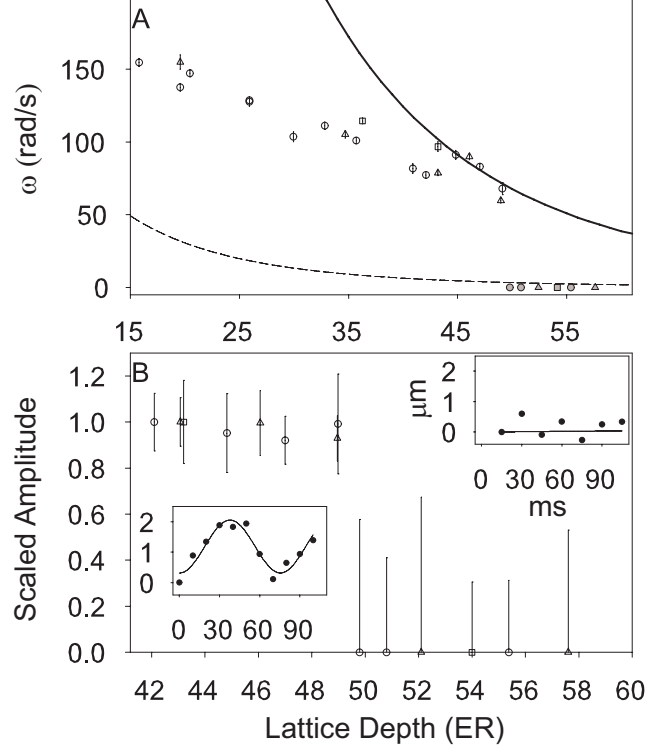


FIG. 5:

(A) Center-of-mass oscillation frequency, ω , vs. lattice depth for harmonic trap displacements $\Delta = 6.4 \mu\text{m}$ (circles), $4.3 \mu\text{m}$ (triangles), and $3.2 \mu\text{m}$ (squares). The solid line indicates the excitation frequencies for a lattice array phonon mode with an effective length of 4 sites, and the dashed line denotes the oscillation frequency predicted by the semiclassical hydrodynamic equations. Filled points, shown with $\omega = 0$, represent data where we cannot experimentally resolve an oscillation.

(B) Center-of-mass oscillation amplitude vs. lattice depth. Typical oscillation sequences are shown in the upper and lower insets, for parameters $U = 54 E_R$, $\Delta = 6.4 \mu\text{m}$ and $U = 47 E_R$, $\Delta = 6.4 \mu\text{m}$ respectively. Below the transition, errors are inferred from the residuals of the non-linear least squares fits. Above the transition, error bars are determined from the variance of the ensemble of data points. Amplitudes are scaled to the measured oscillation amplitude for $U = 42 E_R$.

This work was supported by the National Science Foundation, the Army Research Office and the Office of Naval Research. S. D. acknowledges support from the German Academic Exchange Service (DAAD). We thank A. Fetter, T.L. Ho, S. Sachdev, S. Girvin, and A. Polkovnikov for useful discussions and C. Orzel and M. Fenselau for experimental contribu-

tions during the early stages of this work.

-
- [1] *The Physics of Quantum Information: Quantum Cryptography, Quantum Teleportation, Quantum Computation*, D. Bouwmeester, A. Ekert, A. Zeilinger, Eds. (Springer-Verlag, Berlin, 2000).
- [2] M. A. Nielsen, I. L. Chuang, *Quantum Computation and Quantum Information* (Cambridge Univ. Press, Cambridge, 2000).
- [3] D. Vion et al., *Science* **296**, 886 (2002).
- [4] P. Bouyer and M.A. Kasevich, *Phys. Rev. A* **56**, R1083 (1997).
- [5] G. Paraoanu, S. Kohler, F. Sols and A. Leggett, *J. Phys. B* **34**, 4689 (2001).
- [6] K. Burnett, M. Edwards, C. Clark and M. Shotton, *J. Phys. B* **35**, 1671 (2002).
- [7] M.P.A. Fisher, P.B. Weichman, G. Grinstein, D.S. Fisher, *Phys. Rev. B* **40**, 546 (1989).
- [8] M. Greiner, O. Mandel, T. Esslinger, T. Hänsch, I. Bloch, *Nature* **415**, 39 (2002).
- [9] R. Bradley and S. Doniach, *Phys. Rev. B* **30**, 1138 (1984).
- [10] C. Orzel, A.K. Tuchman, M.L. Fenselau, M. Yasuda, M.A. Kasevich, *Science* **291**, 2386 (2001).
- [11] F. Gerbier et al., *Phys. Rev. Lett.* **95**, 050404 (2005).
- [12] R. Roth and K. Burnett, *Phys. Rev. A* **67**, 031602 (2003).
- [13] F. S. Cataliotti et al., *Science* **293**, 843 (2001).
- [14] L. Fallani et al., *Phys. Rev. Lett.* **93**, 140406 (2004).
- [15] C. Fertig et al., *Phys. Rev. Lett.* **94**, 120403 (2005).
- [16] T. Stöferle, H. Moritz, C. Schori, M. Köhl, T. Esslinger, *Phys. Rev. Lett.* **92**, 130403 (2004).
- [17] L. J. Geerligs, M. Peters, L. E. M. de Groot, A. Verbruggen, J. E. Mooij, *Phys. Rev. Lett.* **63**, 326 (1989).
- [18] D. Jaksch, C. Bruder, J.I. Cirac, C.W. Gardiner, and P. Zoller, *Phys. Rev. Lett.* **81**, 3108 (1998).
- [19] $\gamma \equiv \int d^3r \phi_i(r) \left(-\frac{\hbar^2}{2m} \nabla^2 + U(r) \right) \phi_j(r)$ and $\beta_i \equiv \int d^3r \phi_i^2 \phi_i^2$, where $\phi_{i,j}$ are nearest neighbor single-particle states, and $U(r)$ is the external potential. γ was determined numerically from a band structure calculation. In the limit of large U , our numerical values match the analytic result $\gamma = (8E_R/\pi)(U/E_R)^{3/4} e^{-2\sqrt{U/E_R}}$ [Y. Castin, PhD thesis, Université Paris VI (1992)].
- [20] S. Sachdev, *Quantum Phase Transitions* (Cambridge University Press, New York, 1999) Chap-

ter 10.

- [21] N. Elstner and H. Monien, Phys. Rev. B **59**, 12184 (1999).
- [22] V. Kashurnikov, N. Prokofev, B. Svistunov, Phys. Rev. A. **66**, 31601 (2002).
- [23] A. Polkovnikov, S. Sachdev, S. Girvin, Phys. Rev. A **66**, 53607 (2002).
- [24] G. Batrouni et al., Phys. Rev. Lett. **89**, 117203 (2002).
- [25] G. Campbell et al., Science **313**, 649 (2006).
- [26] F. Gerbier, S. Fölling, A. Widera, O. Mandel, I. Bloch, Phys. Rev. Lett. **96**, 090401 (2006).
- [27] G. Baym and C. Pethick, Phys. Rev. Lett. **76**, 6 (1996).
- [28] I. Zapata, F. Sols, A. Leggett, Phys. Rev. A **57**, R28 (1998).
- [29] D. van Oosten, P. van der Staten, H. Stoof, Phys. Rev. A **67**, 033606 (2003).
- [30] J. Denschlag et al., J. Phys. B **35**, 3905 (2002).
- [31] We apply the transient phase gradient by suddenly switching the magnitude of the rotating component, B_{rot} , of the TOP magnetic field. Since the curvature of a TOP trap scales as B_q^2/B_{rot} , a sudden increase in B_{rot} weakens the magnetic trap and the atoms are exposed to a gravity-induced potential gradient along the vertical array. For large enough values of B_{rot} , gravity imprints a potential energy difference $mg\lambda/2$ between adjacent wells for the duration τ of the pulse. If the phase in each well is defined, it precesses as $\phi_j = \phi_{j_0} + mg(j\lambda/2)\tau$ where all initial phases ϕ_{j_0} are equal.
- [32] A. Smerzi, A. Trombettoni, P. Kevrekidis, A. Bishop Phys. Rev. Lett. **89**, 170402 (2002).
- [33] J. Javanainen, Phys. Rev. A **60**, 4902 (1999).
- [34] L. Isella and J. Ruostekoski, Phys. Rev. A **72**, 011601(R) (2005).
- [35] M. Kramer, L. Pitaevskii, S. Stringari, Phys. Rev. Lett. **88**, 180404 (2002).
- [36] J. Ruostekoski and L. Isella, Phys. Rev. Lett. **95**, 110403 (2005).
- [37] F. Ferlaino et al., Phys. Rev. A **66**, 011604 (2002).
- [38] C. Kollath, U. Schollwöck, J. von Delft, and W. Zwerger, Phys. Rev. A **69**, 031601(R) (2004).
- [39] In particular $\int u_q^2 - v_q^2 = 0$ rather than 1 in this regime, where u_q and v_q are the quasiparticle creation and annihilation operators. See, A. Fetter in in *Proceedings of the International School of Physics "Enrico Fermi," Course CXL*, M. Inguscio, S. Stringari, C. Wieman Eds. (IOS Press, Amsterdam, 1999), pp. 201 - 263.
- [40] Y. Castin, R. Dum, Phys. Rev. Lett. **79**, 3553 (1997).
- [41] J. Anglin, A. Vardi, Phys. Rev. A **64**, 013605 (2001).

- [42] A. Smerzi, S. Fantoni, S. Giovanazzi, S.R. Shenoy Phys. Rev. Lett. **79**, 4950 (1997).
- [43] For a general overview, see A. Leggett, Rev. Mod. Physics **73**, 307 (2001), section VII.D.